Biomass Conversion and Biorefinery
https://doi.org/10.1007/s13399-022-02961-9

ORIGINAL ARTICLE

Dynamic pathways for the bioconvection in thermally activated rotating system

Noor Saeed Khan[3] · Usa Wannasingha Humphries[4] · Wiyada Kumam[5] · Poom Kumam[1,2] · Taseer Muhammad[6]

Received: 30 March 2022 / Revised: 10 June 2022 / Accepted: 15 June 2022

Abstract
This article communicates Cattaneo-Christov heat and mass flux theory in the flow of Maxwell nanofluid and gyrotactic microorganisms towards a spinning disk with the effects of Hall current, and Darcy porous medium. Entropy generation is also taken into account in the presence of Brownian motion, thermophoresis, thermal radiation, heat source/sink, and chemical reaction. Non-dimensional equations are derived for the velocities, temperature, nanoparticles concentration, and motile gyrotactic microorganisms concentration with the help of similarity transformations. Homotopy analysis method (HAM) is used to obtain the solution. Graphs and a table are plotted to show the effects of physical parameters. Numerical computations are given to analyze the values of skin friction coefficients which present a nice agreement with the published results.

Keywords Cattaneo-Christov heat and mass flux theory · Maxwell nanofluid · Gyrotactic microorganisms · Entropy generation · Homotopy analysis method

Nomenclature

m	Hall parameter
(u, v, w)	Velocity components
(r, ϑ, z)	Cylindrical coordinates
a	Stretching rate
Sc	Schmidt number
k_r	Dimensional chemical reaction parameter
k_c	Non-dimensional chemical reaction parameter
M	Magnetic field parameter
Pr	Prandtl number
E'''_{gen}	Entropy generation
E'''_0	Characteristic entropy generation
N_G	Non-dimensional entropy generation rate
Le	Lewis number
Pe	Peclet number
Nb	Brownian motion parameter
Nt	Thermophoresis parameter
R	Ideal gas constant
Br	Brinkman number
C_i, $i = 1, 2, 3..., 11$	Arbitrary constants
Re	Reynolds number

✉ Noor Saeed Khan
noorsaeedkhankhattak@gmail.com

✉ Usa Wannasingha Humphries
usa.wan@kmutt.ac.th

✉ Poom Kumam
poom.kum@kmutt.ac.th

1 KMUTTFixed Point Research Laboratory, Room SCL 802 Fixed Point Laboratory, Science Laboratory Building, Department of Mathematics, Faculty of Science, King Mongkut's University of Technology Thonburi (KMUTT), Bangkok 10140, Thailand

2 Center of Excellence in Theoretical and Computational Science (TaCS-CoE), Science Laboratory Building, Faculty of Science, King Mongkut's University of Technology Thonburi (KMUTT), 126 Pracha-Uthit Road, Bang Mod, Thung Khru, Bangkok 10140, Thailand

3 Department of Mathematics, Division of Science and Technology, University of Education, Lahore 54000, Pakistan

4 Department of Mathematics, Faculty of Science, King Mongkut's University of Technology Thonburi (KMUTT), 126 Pracha Uthit Road, Bang Mod, Thung Khru, Bangkok 10140, Thailand

5 Program in Applied Statistics, Department of Mathematics and Computer Science, Faculty of Science and Technology, Rajamangala University of Technology Thanyaburi (RMUTT), Pathum Thani 12110, Thailand

6 Department of Mathematics, College of Sciences, King Khalid University, Abha 61413, Saudi Arabia

T	Temperature
C	Nanoparticles concentration
N	Motile microorganisms concentration
P	Pressure
c_P	Specific heat at constant pressure
D_B	Diffusivity
B	Chemical species
$f'(\zeta)$	Dimensionless radial velocity
$g(\zeta)$	Dimensionless azimuthal velocity
$h(\zeta)$	Dimensionless axial velocity
B_0	Applied magnetic field strength
$\boldsymbol{L}$	Linear operator

Greek symbols

Ω	Angular velocity
σ	Electrical conductivity
ψ	Stream function
ζ	Similarity variable
$\phi(\zeta)$	Dimensionless nanoparticles concentration
$\theta(\zeta)$	Dimensionless temperature
$\chi(\zeta)$	Dimensionless gyrotactic microorganisms concentration
λ_1	Relaxation time parameter
γ_1	Thermal relaxation time parameter
γ_2	Mass relaxation time parameter
γ_3	Non-dimensional thermal relaxation time parameter
γ_4	Non-dimensional solutal time relaxation parameter
γ_5	Gyrotactic microorganisms concentration difference parameter
γ_6	Temperature difference parameter
γ_7	Diffusion constant parameter
ν	Kinematic viscosity
μ	Dynamic viscosity
ρ	Density
α	Thermal diffusivity
Ω_1	Dimensionless stretching parameter

Subscripts

f	Base fluid

Superscripts

$'$	Differentiation with respect to ζ

1 Introduction

Non-Newtonian fluids have applications in concentrated products, including fabrics carbon, glass, and paints. Researchers have keen interest in the investigations of non-Newtonian fluids. Wang et al. [1] used the ramped conditions and three different types of definitions of fractional differential operators, namely Caputo, Caputo-Fabrizio, and Atangana-Baleanu to analyze the Oldroyd-B nanofluid in a porous medium. Farooq et al. [2] explored the characteristics of bioconvection in Carreau nanofluid flow with Cattaneo-Christov heat and mass transfer in the presence of thermal radiation, activation energy, Brownian motion, and thermophoresis. Alzahrani et al. [3] investigated the convective micropolar fluid through a porous nonlinear stretching sheet with variable thickness using the numerical second-order finite difference method, namely the Keller-box scheme. Ahmad et al. [4] examined the steady bio-convective hybridized micropolar nanofluid flow with the stratification conditions above a vertical exponentially stretching surface to analyze the heat and mass transfer rate, activation energy using Cattaneo-Christov heat flux theory. The non-Newtonian behaviors with other characteristics of fluids and heat transfer can be seen in the references [5–14].

Nanofluid is a subclass of liquid consisting of nanometer-sized (1–100 nm) materials, known as nanoparticles. Nanofluid describes the suspended nano-materials in the conventional liquid to enhance the thermal conduction. The nanoparticle use has drawn the attention of investigators in present time due to their remarkable role in the fields of mechanical science, electronics, food processing, biology, medicine, and biomaterials. The targeted drug delivery and cancer treatment hypotheses, fermentation process, nanotechnologies, and medication are also dependent on the applications of the nanofluids. It is a fact that in a refrigerator and other devices, fluid passages through the microfluidics are completely dependent on the heat transporting particles. So nanofluid dynamics is the main term to be understood in all disciplines concerned with nanoparticles suspensions. Khan et al. [15] focused on the boundary layer flow of hybrid nanofluid with gyrotactic microorganisms and porous medium across the rotating disk by considering the double diffusion theory, Joule heating effect, chemical reaction, and multiple slip boundary conditions. Ahmad et al. [16] discussed the unsteady three-dimensional bio-convective Maxwell nanofluid flow through an exponentially stretched sheet with the convective boundary conditions by using Matlab's bvp4c function. In another study, Ahmad et al. [17] examined the two different nanoparticles that offer better heat transfer performance and thermophysical properties than traditional heat transfer fluids (water, oil, and refrigerant-134A) and nanofluid with single nanoparticles. Similarly, investigating the nanofluid, Ahmad et al. [18] worked on the unsteady bio-convective hybridized micropolar nanofluid flow over vertical exponentially stretching surface under the stratification conditions with the involvement of Cattaneo-Christov heat flux and activation energy. Khan et al. [38] analyzed bioconvection nanofluid flow and entropy generation in rotating system with the application of Homotopy Analysis Method. Some relevant materials can be studied in the references [39–43].

Bioconvection is an interesting process of materials associated with the swimming of microorganisms. The phenomenon of bioconvection performs a key role in the production of biochemical oils and meteorological applications including heated spring colonized through motile gyrotactic microorganisms termed as thermopile. Ramesh et al. [44] considered the applications of nano-particles and bioconvection in the flow of Maxwell nanofluid along with swimming of gyrotactic microorganisms configured by a Riga surface in the presence of thermal radiation, activation energy and the convective-Nield boundary conditions. Liu [45] scrutinized the MHD Maxwell nanofluid flow over an extended cylinder with nonlinear thermal radiation amalgamated with chemical reaction in a Darcy-Forchheimer porous medium and gyrotactic microorganisms. Ramzan et al. [46] discussed the new mathematical model of three-dimensional tangent hyperbolic nanofluid flow with Hall current and ion slip in the presence of modified Fourier law with Newtonian heating, Arrhenius activation energy, chemical reaction, and gyrotactic microorganisms. Song et al. [47] reported the stagnation point flow of radiative micropolar nanofluid over an off-centered rotating disk with applications of motile microorganisms incorporating the novel dynamic of thermal radiation and activation energy. Investigating bioconvection, Song et al. [48] communicated the thermal assessment of Sutterby nanofluid containing the gyrotactic microorganisms with solutal and Marangoni boundaries, melting phenomenon, and thermal conductivity. Abdal et al. [49] analyzed the flow of Maxwell nanofluid over an extending sheet with bioconvection of micron size self-motivated organisms, radiative heat flux, and two temperature boundary conditions, namely, prescribed surface temperature (PST) and prescribed heat flux (PHF) under the influence of magnetic field and porosity. Chu et al. [50] highlighted the newly developed concept of Rosseland approximation and gyrotactic microorganisms in steady, two-dimensional, incompressible flow of Walter's-B nanofluid over a stretched surface. The other studies related to bioconvection can be seen in [51–60].

All the above cited papers have remarkable investigations about different fluid flows with heat and mass transfer describing the various charateristics of fluids and effects of parameters on these flows. However, still there is a gap to investigate the Hall current and Darcy Forchheimer porous medium effects with entropy generation as well as gyrotactic microorganisms in rotating system for non-Newtonian nanofluid. The current study presents the investigation about Hall current effect, porosity, and entropy generation in the Maxwell nanofluid flow past a stretchable rotating disk in the presence of Cattaneo-Christov heat and mass flux theory. The problem is mathematically modeled and then solved through an analytical technique [61, 62].

2 Methods

2.1 Basic equations

The steady axisymmetric swirling flow of incompressible Maxwell nanofluid containing nanoparticles and motile gyrotactic microorganisms in the presence of Hall current effect and entropy generation is investigated. The Cattaneo-Christov theory is applied for the heat and mass transfer by assuming the flow in the upper plane $z \geq 0$, with uniform angular velocity, stretching rate, constant temperature, nanoparticles concentration, and motile gyrotactic microorganisms concentration as Ω, a, T_w, C_w, and N_w respectively while at the free stream, the temperature, nanoparticles concentration, and motile gyrotactic microorganisms concentration are T_∞, C_∞, and N_∞ respectively. Magnetic field is applied with the power B_0 along with the z-direction (please see Fig. 1). For the life of microorganisms, water is taken as the base fluid.

Following the above assumptions, governing equations for the conservation of total mass, flow, heat transfer, nanoparticles concentration, and motile microorganisms are presented as in [23, 24, 38].

$$\frac{\partial u}{\partial r} + \frac{u}{r} + \frac{\partial w}{\partial z} = 0, \tag{1}$$

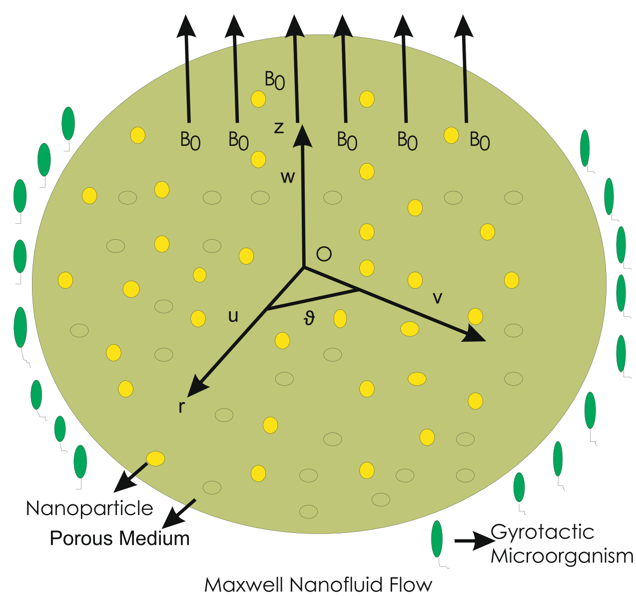

Fig. 1 Physical configuration of the problem

$$\rho_f\left(u\frac{\partial u}{\partial r}+w\frac{\partial u}{\partial z}-\frac{v^2}{r}\right)=\mu_f\frac{\partial^2 u}{\partial z^2}-\lambda_1\left[u^2\frac{\partial^2 u}{\partial r^2}+w^2\frac{\partial^2 u}{\partial z^2}+2uw\frac{\partial^2 u}{\partial r\partial z}-\frac{2uv}{r}\frac{\partial v}{\partial r}-\frac{2vw}{r}\frac{\partial v}{\partial z}+\frac{uv^2}{r^2}+\frac{v^2}{r}\frac{\partial u}{\partial r}\right] -\frac{\sigma_f B_0^2(u-mv+w\lambda_1\frac{\partial u}{\partial z})}{1+m^2}-\frac{\mu_f}{k}u-k^F u^2, \tag{2}$$

$$\rho_f\left(u\frac{\partial v}{\partial r}+w\frac{\partial v}{\partial z}+\frac{1}{r}uv\right)=\mu_f\frac{\partial^2 v}{\partial z^2}-\lambda_1\left[u^2\frac{\partial^2 v}{\partial r^2}+w^2\frac{\partial^2 v}{\partial z^2}+2uw\frac{\partial^2 v}{\partial r\partial z}+\frac{2uv}{r}\frac{\partial u}{\partial r}+\frac{2vw}{r}\frac{\partial u}{\partial z}-\frac{2u^2}{r^2}-\frac{v^3}{r^2}+\frac{v^2}{r^2}\frac{\partial v}{\partial r}\right] -\frac{\sigma_f B_0^2(v+mu+w\lambda_1\frac{\partial v}{\partial z})}{1+m^2}-\frac{\mu_f}{k}w-k^F w^2, \tag{3}$$

$$\left(u\frac{\partial T}{\partial r}+w\frac{\partial T}{\partial z}\right)=\frac{\alpha}{\rho c_P}\frac{\partial^2 T}{\partial z^2}+2\gamma_1\tau\frac{D_T}{T_\infty}\left[u\frac{\partial T}{\partial z}\frac{\partial^2 T}{\partial r\partial z}+w\frac{\partial T}{\partial z}\frac{\partial^2 T}{\partial z^2}\right]+\tau\left[D_B\left(\frac{\partial T}{\partial z}\frac{\partial C}{\partial z}\right)+\frac{D_T}{T_\infty}\left(\frac{\partial T}{\partial z}\right)^2\right] +\frac{Q_0}{\rho c_P}(T-T_\infty)+\gamma_1\frac{Q_0}{\rho c_P}\left(u\frac{\partial T}{\partial r}+w\frac{\partial T}{\partial z}\right)+\gamma_1\tau D_B\left[u\frac{\partial T}{\partial z}\frac{\partial^2 C}{\partial r\partial z}+u\frac{\partial C}{\partial z}\frac{\partial^2 T}{\partial r\partial z}+w\frac{\partial T}{\partial z}\frac{\partial^2 C}{\partial z^2}+w\frac{\partial C}{\partial z}\frac{\partial^2 T}{\partial z^2}\right] +\gamma_1\left[u\frac{\partial w}{\partial r}\frac{\partial T}{\partial z}+u\frac{\partial u}{\partial r}\frac{\partial T}{\partial r}+w\frac{\partial u}{\partial z}\frac{\partial T}{\partial r}+w\frac{\partial w}{\partial z}\frac{\partial T}{\partial z}+u^2\frac{\partial^2 T}{\partial r^2}+w^2\frac{\partial^2 T}{\partial z^2}+2uw\frac{\partial^2 T}{\partial r\partial z}\right], \tag{4}$$

$$u\frac{\partial C}{\partial r}+w\frac{\partial C}{\partial z}=D_B\frac{\partial^2 C}{\partial z^2}+\gamma_2\tau\frac{D_T}{T_\infty}\left[u\frac{\partial^3 T}{\partial r\partial z^2}+w\frac{\partial^3 T}{\partial z^3}\right]+\frac{D_T}{T_\infty}\frac{\partial^2 T}{\partial z^2}-k_r(C-C_\infty)+\gamma_2 k_r\left(u\frac{\partial C}{\partial r}+w\frac{\partial C}{\partial z}\right) -\gamma_2\left[u\frac{\partial w}{\partial r}\frac{\partial C}{\partial z}+u\frac{\partial u}{\partial r}\frac{\partial C}{\partial r}+w\frac{\partial u}{\partial z}\frac{\partial C}{\partial r}+w\frac{\partial w}{\partial z}\frac{\partial C}{\partial z}+u^2\frac{\partial^2 C}{\partial r^2}+w^2\frac{\partial^2 C}{\partial z^2}+2uw\frac{\partial^2 C}{\partial r\partial z}\right], \tag{5}$$

$$u\frac{\partial N}{\partial r}+w\frac{\partial N}{\partial z}+\frac{bW_c}{(C_w-C_\infty)}\frac{\partial}{\partial z}\left(N\frac{\partial C}{\partial z}\right)=D_n\left[\frac{\partial^2 N}{\partial r^2}+\frac{1}{r}\frac{\partial N}{\partial r}+\frac{\partial^2 N}{\partial z^2}\right], \tag{6}$$

using the boundary conditions

$$u=ra,\quad v=r\Omega,\quad w=0,\quad T=T_w,\quad C=C_w,\quad N=N_w\quad at\quad z=0, \tag{7}$$

$$u\to 0,\quad v\to 0,\quad T\to T_\infty,\quad C\to C_\infty,\quad N\to N_\infty\quad as\quad z\to\infty, \tag{8}$$

where $u(r,\vartheta,z)$, $v(r,\vartheta,z)$ and $w(r,\vartheta,z)$ are the velocity components, P is the pressure, $B=(0,0,\mathrm{B}_0)$ is the magnetic induction, and m is the Hall parameter [38]. λ_1 is the relaxation time parameter. γ_1 and γ_2 are the thermal relaxation time and mass relaxation time parameters respectively. α is the thermal diffusivity, k is the permeability of porous medium, and $k^F=\frac{C_b}{\sqrt{k}}$ is the Forchheimer resistance factor in which C_b is the drag coefficient. D_B and D_T are the Brownian and thermophoretic diffusion coefficients, ρ_f, μ_f, σ_f and $(c_p)_f$ are the density, effective dynamic viscosity, electrical conductivity, and heat capacitance of the nanofluid respectively. $\nu_f=\frac{\mu_f}{\rho_f}$ is the kinematic viscosity, $\tau=\frac{(\rho c)_P}{(\rho c)_f}$ is the ratio of heat capacity of nanoparticles to heat capacity of nanofluid, Q_0 is the heat generation source parameter, k_r is the chemical reaction rate, b is the chemotaxis constant, W_c is the maximum cell swimming speed, and D_n is the diffusivity of microorganisms.

In order to make the above governing Eqs. (1–9) dimensionless, the following transformations are introduced

$$u=r\Omega f(\zeta),\ v=r\Omega g(\zeta),\ w=(\Omega\nu_f)^{\frac{1}{2}}h(\zeta),\quad \theta(\zeta)=\frac{T-T_\infty}{T_w-T_\infty},\ \phi(\zeta)=\frac{C-C_\infty}{C_w-C_\infty},\quad \chi(\zeta)=\frac{N-N_\infty}{N_w-N_\infty},\ \zeta=\left[\frac{\Omega}{\nu_f}\right]^{\frac{1}{2}}z. \tag{9}$$

Substituting the values from Eqs. (9) in (1–8), the following eight Eqs. (10–17) are obtained.

$$2f+h'=0, \tag{10}$$

$$f^2-g^2+f'h-f''+\beta_1\left(h^2f''+2ff'h-2gg'h\right)-\frac{M(f'-mg-2\beta_1 hf')}{1+m^2}-\lambda_3 f-\lambda_4 f^2=0, \tag{11}$$

$$2fg + g'h - g'' + \beta_1 \left(g''h^2 + 2\left(fg' + f'g\right)h\right) - \frac{M(mf' + g - 2\beta_1 hg')}{1 + m^2} - \lambda_3 g - \lambda_4 g^2 = 0, \tag{12}$$

$$\frac{1}{Pr}\theta'' - h\theta' + Nb\left(\theta'\phi' + \gamma_3\left(h\theta'\phi'' + h\theta''\phi'\right)\right) + Nt\left((\theta')^2 + 2\gamma_3 h\theta'\theta''\right) - \gamma_3\left(h^2\theta'' + hh'\theta'\right)\beta_2\theta + \gamma_3\beta_2 h\theta' = 0, \tag{13}$$

$$\phi'' - PrLeh\phi' - \gamma_4 PrLe\left(h^2\phi'' + hh'\phi'\right) + \frac{Nt}{Nb}\left(\theta'' + \gamma_4 h\theta'''\right) - PrLek_c\phi - PrLek_c h\phi' = 0, \tag{14}$$

$$\chi'' - Lbh\chi' - Pe\left(\chi'\phi' + \phi''(\gamma_5 + \chi)\right) = 0, \tag{15}$$

$$f = \Omega_1, g = 1, h = 0, \theta = 1, \phi = 1, \chi = 1 \quad at \quad \zeta = 0, \tag{16}$$

$$f \to 0, g \to 0, h \to 0, \theta \to 0, \phi \to 0, \chi \to 0 \quad as \quad \zeta \to \infty, \tag{17}$$

where ($'$) represents the differentiability through ζ. $\beta_1 = \lambda_1\Omega$ is the non-dimensional Maxwell nanofluid parameter, $\gamma_3 = \gamma_1\Omega$ is the non-dimensional thermal relaxation time parameter, $\gamma_4 = \gamma_2\Omega$ is the non-dimensional solutal relaxation time parameter, $\Omega_1 = \frac{a}{\Omega}$ is the stretching parameter, $\lambda_3 = \frac{\nu_f}{k\Omega}$ is the porosity parameter, $\lambda_4 = \frac{k^F}{\sqrt{k}}$ is the Darcy Forchheimer parameter, $M = \frac{\sigma_f B_0^2}{\rho_f\Omega}$ is the magnetic field parameter, $Pr = \frac{\nu_f}{\alpha}$ denotes the Prandtl number, $\beta_2 = \frac{Q_0}{(\rho c_P)\Omega}$ is the heat generation parameter, $k_c = k_1\Omega$ is the chemical reaction parameter, $Lb = \frac{\nu_f}{D_n}$ is the bioconvection Lewis number, $Le = \frac{\nu_f}{D_B}$ is the Lewis number, $Pe = \frac{bW_c}{D_n}$ is the Peclet number, $\gamma_5 = \frac{N_\infty}{N_w - N_\infty}$ is microorganisms concentration difference parameter, $Nb = \frac{\tau D_B(C_w - C_\infty)}{\nu_f}$ is the Brownian motion parameter, and $Nt = \frac{\tau D_T(T_w - T_\infty)}{\nu_f T_\infty}$ is the thermophoresis parameter.

The quantities of engineering interest, such as coefficient of skin friction C_F, local Nusselt N_{u_r}, Sherwood number Sh_r, and local motile density number N_{n_r}, are defined as

$$C_F = \frac{\tau|_{z=0}}{\rho_f(r\Omega)^2}, \tag{18}$$

where

$$\tau = \sqrt{(\tau_r)^2 + (\tau_\vartheta)^2}, \tag{19}$$

denotes the sum of shear stresses τ_r and τ_ϑ along radial and transvers directions.

$$Nu_r = \frac{-rq_1}{\alpha(T_w - T_\infty)},\ Sh_r = \frac{-rq_2}{D_B(C_w - C_\infty)},\ Nn_r = \frac{-rq_3}{D_m(N_w - N_\infty)}, \tag{20}$$

where q_1, q_2 and q_3 are the heat, mass, and motile microorganism fluxes at the surface of the rotating disk and are defined as

$$q_1 = -\alpha T_z|_{z=0},\ q_2 = -D_B C_z|_{z=0},\ q_3 = D_m N_z|_{z=0}. \tag{21}$$

Using the information of Eqs. (9) and (18) proceeds to

$$C_F = Re_r^{\frac{-1}{2}}\left[\left(f'(0)\right)^2 + \left(g'(0)\right)^2\right], \tag{22}$$

where $Re_r = \frac{r^2\Omega}{\nu_f}$ is the Reynolds number.

Similarly by putting values from Eqs. (9) in (20), it is obtained that

$$Nu_r = -Re_r^{0.5}\theta'(0),\ Sh_r = -Re_r^{0.5}\phi'(0),\ Nn_r = -Re_r^{0.5}\chi'(0). \tag{23}$$

3 Entropy generation

Through fluid mechanics, in system and its surroundings, entropy generation measures the rate of disorderness. It is related with the friction of particles and kinetic and potential energies. The entropy generation has the equation [51]

$$\begin{aligned} E'''_{gen} = {} & \left(\frac{\partial T}{\partial z}\right)^2 \frac{\alpha}{T_\infty^2} + \frac{1}{T_\infty}\left[\left(\frac{\partial u}{\partial z}\right)^2 + \left(\frac{\partial v}{\partial z}\right)^2\right] \\ & + \left(\frac{\partial C}{\partial z}\right)^2 \frac{RD}{C_\infty} + \left[\frac{\partial C}{\partial z}\frac{\partial T}{\partial z}\right]\frac{RD}{T_\infty} + \left(\frac{\partial N}{\partial z}\right)^2 \frac{RD}{N_\infty} \\ & + \left[\frac{\partial N}{\partial z}\frac{\partial C}{\partial z}\right]\frac{RD}{T_\infty} + \frac{\sigma_f B_0^2(u^2 + v^2)}{1 + m^2}, \end{aligned} \tag{24}$$

where R is the ideal gas constant while D is the diffusivity.

Table 1 Numerical information for the comparison of the present work

Profiles	Ahmed et al. [62]	Present results
$f'(0)$	0.5000776	0.5000775
$g'(0)$	0.6185207	0.6185208
$\theta'(0)$	0.9300460	0.9300461

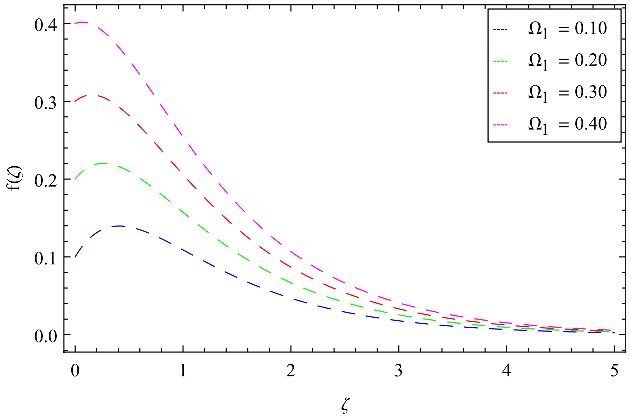

Fig. 2 Behavior of profile against parameter effect

The characteristic entropy generation is

$$E_0''' = \frac{\alpha(T_w - T_\infty)}{v_f T_\infty}. \tag{25}$$

The non-dimensional entropy generation rate $N_G(\zeta)$ is obtained with the help of Eq. (9) as

$$N_G(\zeta) = \frac{E_{gen}'''}{E_0'''}. \tag{26}$$

So

$$\begin{aligned} N_G(\zeta) &= \gamma_6(\theta')^2 + Br\left[f'^2 + g'^2\right] \\ &+ \gamma_7\theta'\phi' + \gamma_7\frac{\gamma_8}{\gamma_6}(\phi')^2 + \gamma_9\theta'\chi' \\ &+ \gamma_9\frac{\gamma_5}{\gamma_6}(\chi')^2 + \frac{BrM}{1+m^2}\left[f^2 + g^2\right], \end{aligned} \tag{27}$$

where $\gamma_6 = \frac{T_w - T_\infty}{T_\infty}$ is the temperature difference parameter, $Br = \frac{\mu_f r^2 \Omega^2}{\alpha(T_w - T_\infty)}$ is the Brinkman number, $\gamma_7 = \frac{RD(C_w - C_\infty)}{\alpha}$ is the diffusion constant parameter due to nanoparticles concentration, $\gamma_8 = \frac{C_w - C_\infty}{C_\infty}$ is the nanoparticles concentration difference parameter, and $\gamma_9 = \frac{RD(N_w - N_\infty)}{\alpha}$ is the diffusion constant parameter due to microorganisms concentration.

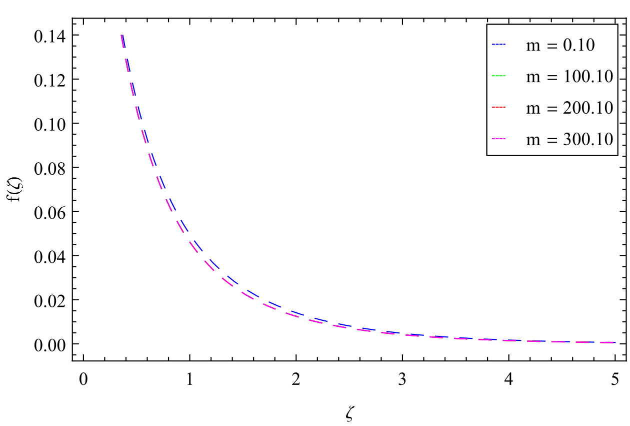

Fig. 3 Behavior of profile against parameter effect

4 Solution methodology

Applying a homotopy analysis method (HAM) [61], the initial approximations and auxiliary linear operators are

$$\begin{aligned} &h_0(\zeta) = 0, f_0(\zeta) = \Omega\exp(-\zeta), g_0(\zeta) = \exp(-\zeta), \\ &\theta_0(\zeta) = \exp(-\zeta), \phi_0(\zeta) = \exp(-\zeta), \chi_0(\zeta) = \exp(-\zeta), \end{aligned} \tag{28}$$

$$\begin{aligned} &\boldsymbol{L}_h = h', \boldsymbol{L}_f = f'' - f', \boldsymbol{L}_g = g'' - g', \boldsymbol{L}_\theta = \theta'' - \theta, \\ &\boldsymbol{L}_\phi = \phi'' - \phi, \boldsymbol{L}_\chi = \chi'' - \chi \end{aligned} \tag{29}$$

The following properties are satisfied with the linear operators

$$\begin{aligned} &\boldsymbol{L}_h\left[C_1\right] = 0, \boldsymbol{L}_f\left[C_2\exp(\zeta) + C_3\exp(-\zeta)\right] = 0, \\ &\boldsymbol{L}_g\left[C_4\exp(\zeta) + C_5\exp(-\zeta)\right] = 0, \\ &\boldsymbol{L}_\theta\left[C_6\exp(\zeta) + C_7\exp(-\zeta)\right] = 0, \\ &\boldsymbol{L}_\phi\left[C_8\exp(\zeta) + C_9\exp(-\zeta)\right] = 0, \\ &\boldsymbol{L}_\chi\left[C_{10}\exp(\zeta) + C_{11}\exp(-\zeta)\right] = 0, \end{aligned} \tag{30}$$

where $C_i (i = 1\text{-}11)$ are the arbitrary constants.

5 Comparsion of the present work with the open literature

For the comparison of the present work, the achieved results for $f'(0)$, $g'(0)$ and $\theta'(0)$ are tabulated in Table 1 which shows the close agreement with [62].

6 Results and discussion

The homotopy analysis method (HAM) is used to solve the non-dimensional Eqs. (10–17) and hence Eq. (27). Parameter effects on the different profiles are shown in the relevant graphs.

Figure 2 shows that by increasing the stretching parameter Ω_1, the radial velocity $f(\zeta)$ is increased. In fact, stretching parameter Ω_1 is the ratio of stretching constant a to the angular velocity Ω. Therefore by the increasing values of stretching parameter Ω_1, the radial velocity $f(\zeta)$ increases due to disk stretching rate. The effect of Hall parameter m is shown in Fig. 3. The high values of m in Eq. (11) for the term $\frac{M(f' - mg - 2\beta_1 hf')}{1+m^2}$ show that radial velocity $f(\zeta)$ is decreased. Figures 4 and 5 reveal the effects of porous and Darcy Forchheimer parameters (λ_3, λ_4) on radial velocity $f(\zeta)$. Fluid motion is enhanced by these two parameters.

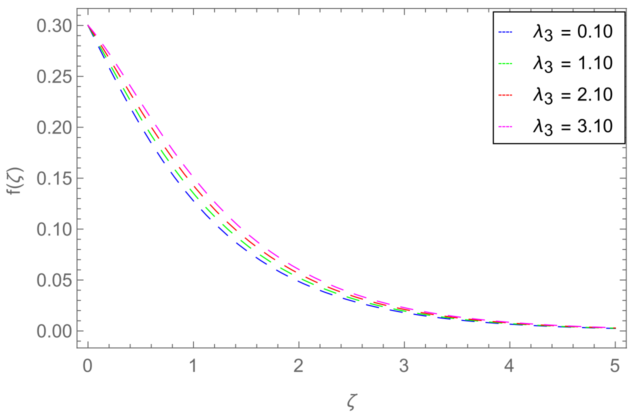

Fig. 4 Behavior of profile against parameter effect

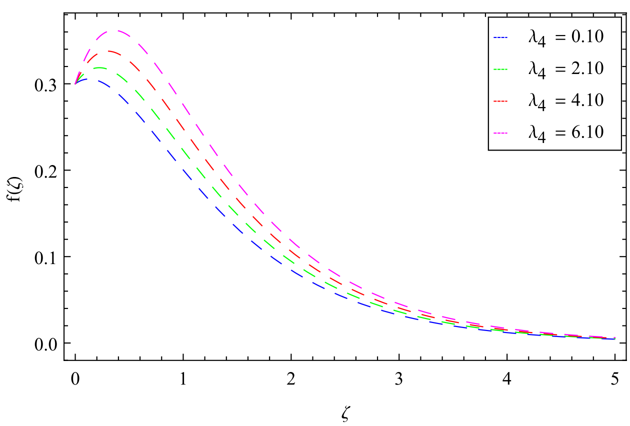

Fig. 5 Behavior of profile against parameter effect

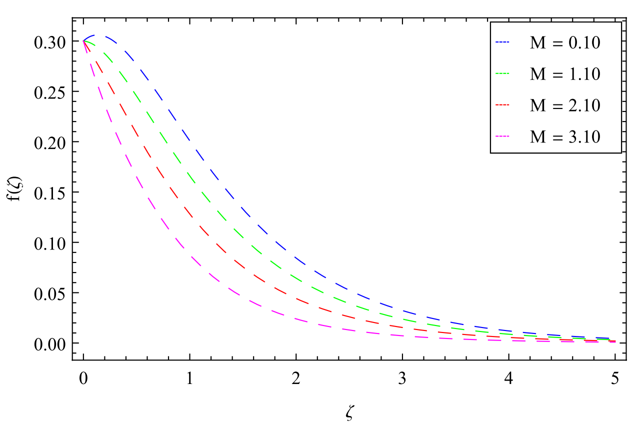

Fig. 6 Behavior of profile against parameter effect

Figure 6 exhibits that the radial velocity $f(\zeta)$ reduces due to magnetic field parameter M. This scenario is on account of Lorentz effect which yields a retarding force along with magnetic field. Figure 7 discloses the role of Maxwell nanofluid parameter β_1 and the radial velocity $f(\zeta)$. The fluid flow

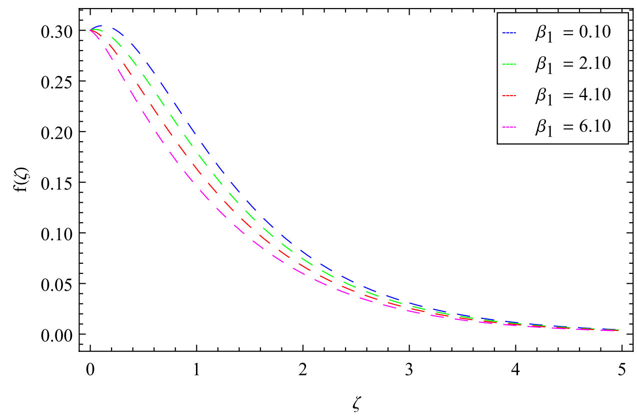

Fig. 7 Behavior of profile against parameter effect

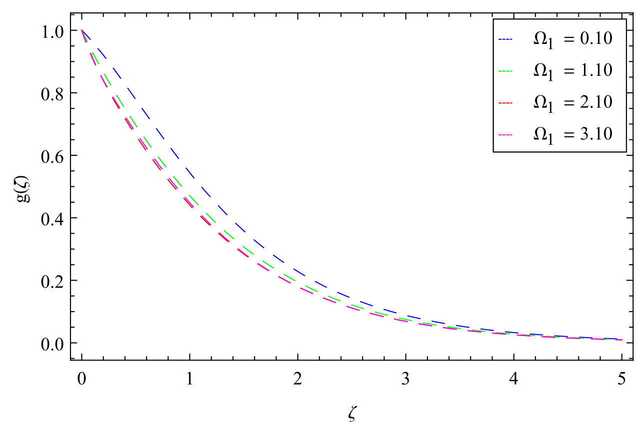

Fig. 8 Behavior of profile against parameter effect

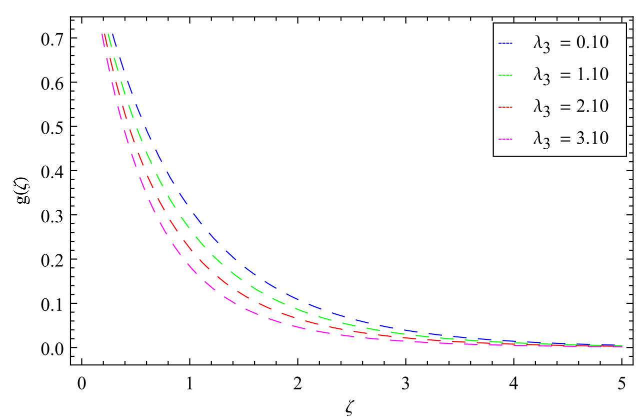

Fig. 9 Behavior of profile against parameter effect

is reduced because for the greater values of β_1, the fluid resumes the form of solid which slows down the motion.

Figure 8 is drawn to show that the azimuthal velocity $g(\zeta)$ is reduced with stretching parameter Ω_1. Similarly in Figs. 9 and 10, it is observed that porous and Darcy Forchheimer parameters have decreasing effects for azimuthal

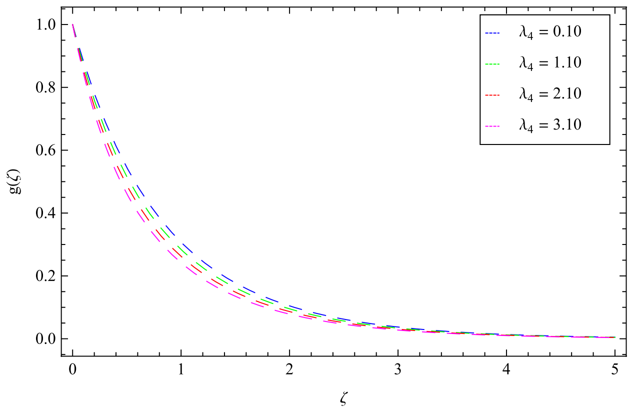

Fig. 10 Behavior of profile against parameter effect

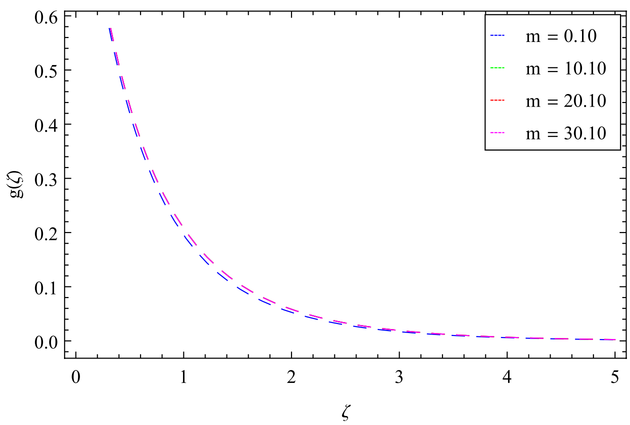

Fig. 11 Behavior of profile against parameter effect

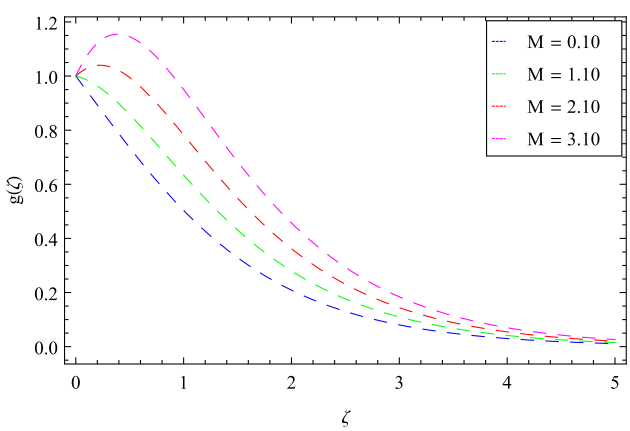

Fig. 12 Behavior of profile against parameter effect

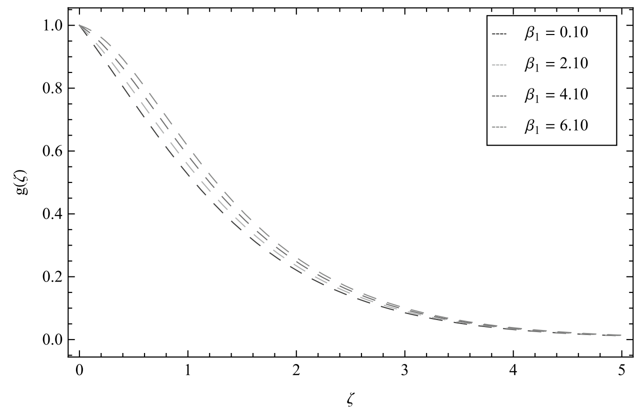

Fig. 13 Behavior of profile against parameter effect

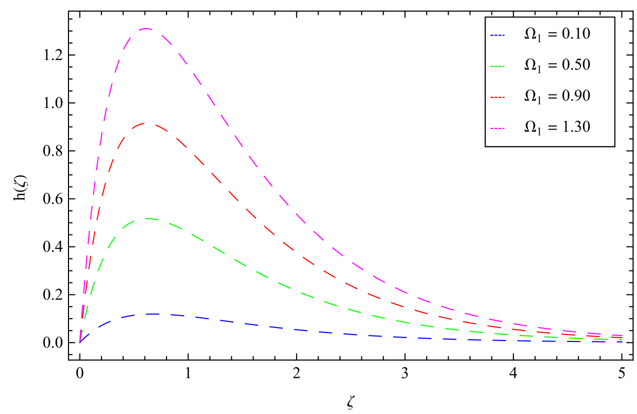

Fig. 14 Behavior of profile against parameter effect

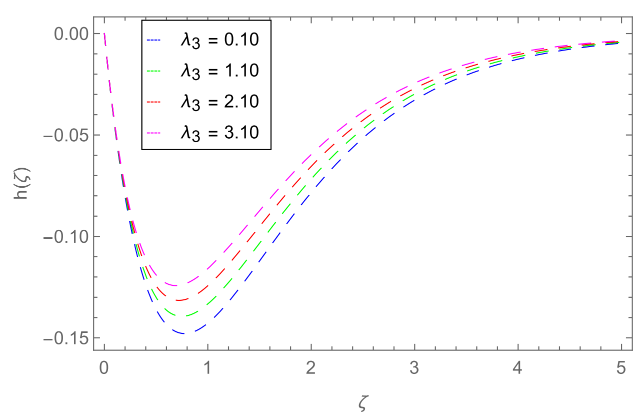

Fig. 15 Behavior of profile against parameter effect

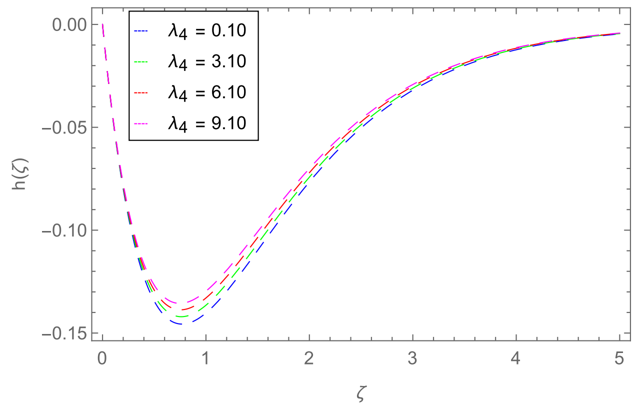

Fig. 16 Behavior of profile against parameter effect

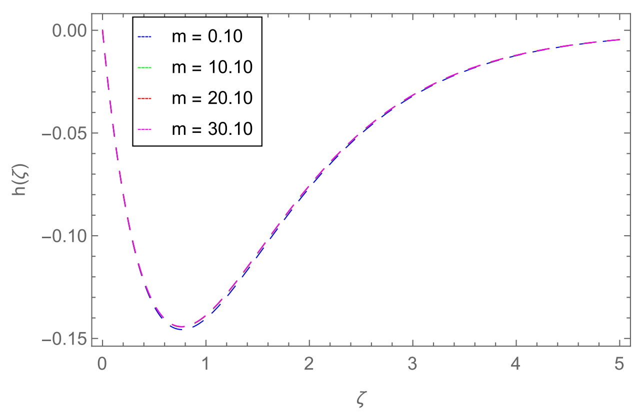

Fig. 17 Behavior of profile against parameter effect

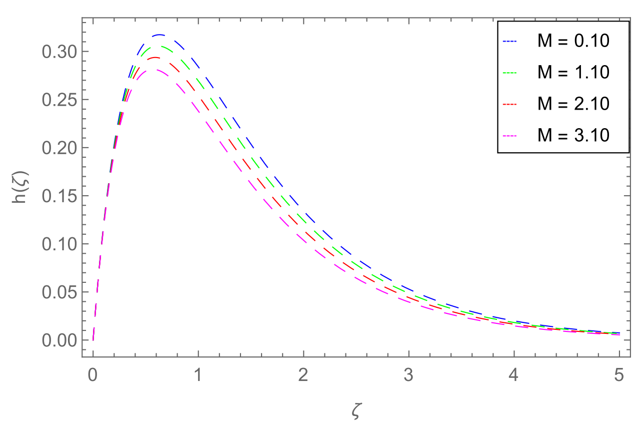

Fig. 18 Behavior of profile against parameter effect

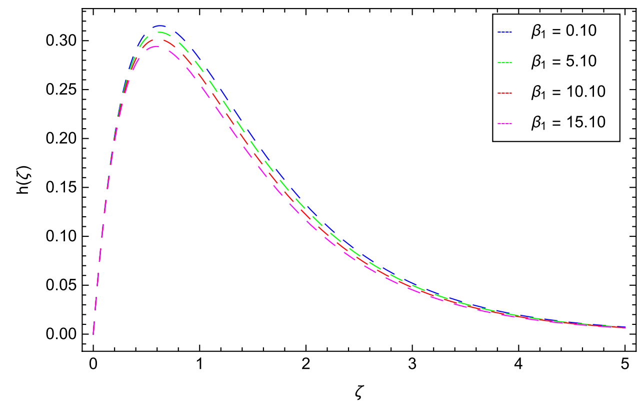

Fig. 19 Behavior of profile against parameter effect

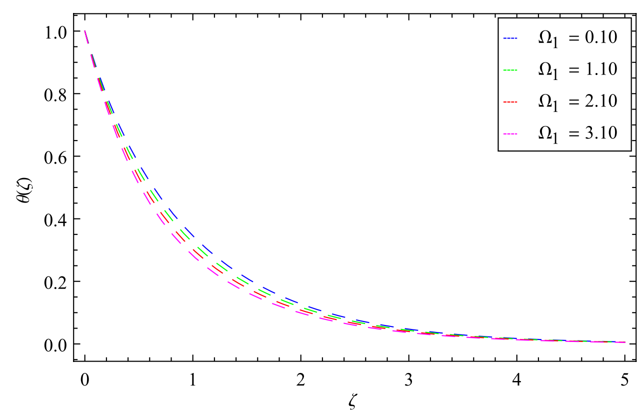

Fig. 20 Behavior of profile against parameter effect

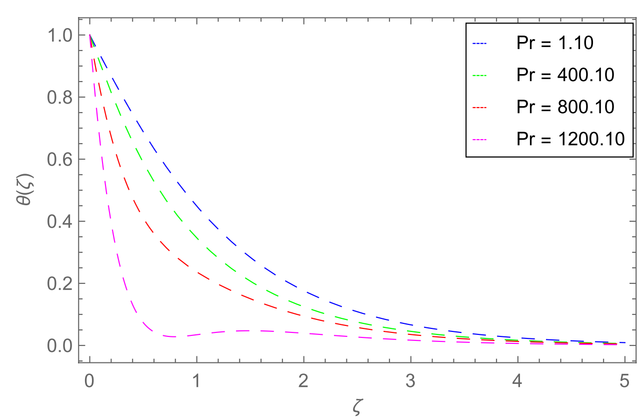

Fig. 21 Behavior of profile against parameter effect

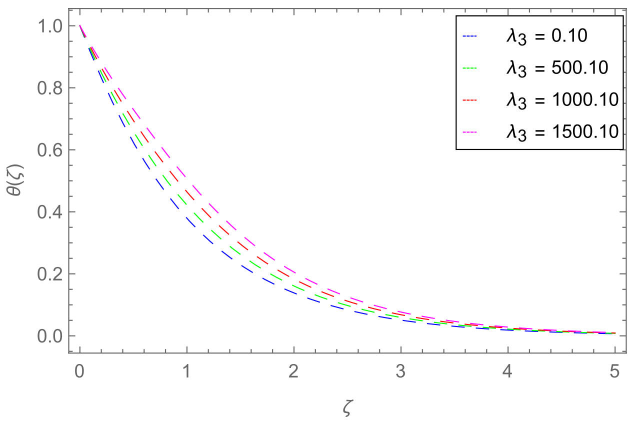

Fig. 22 Behavior of profile against parameter effect

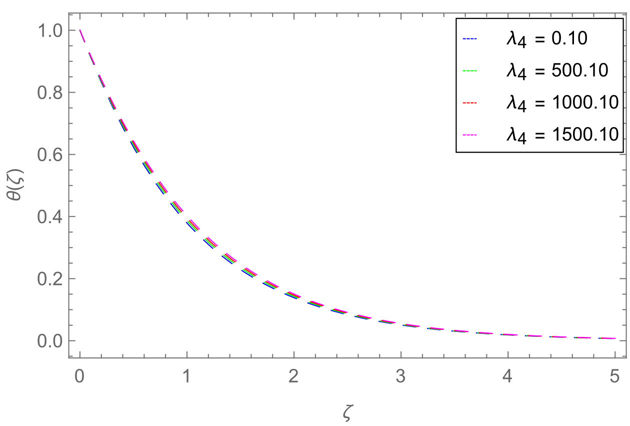

Fig. 23 Behavior of profile against parameter effect

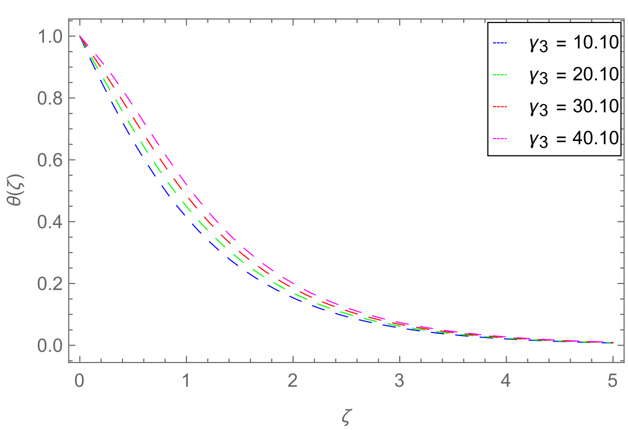

Fig. 24 Behavior of profile against parameter effect

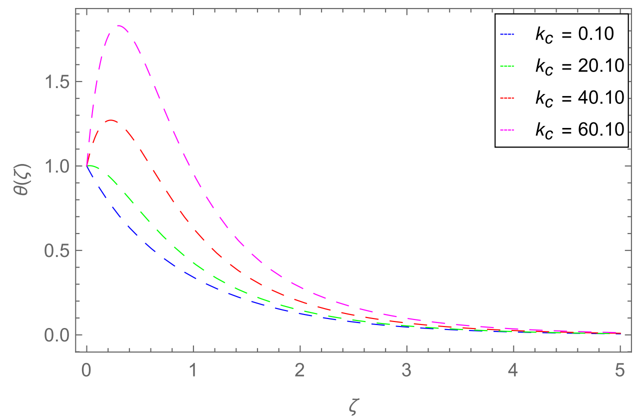

Fig. 25 Behavior of profile against parameter effect

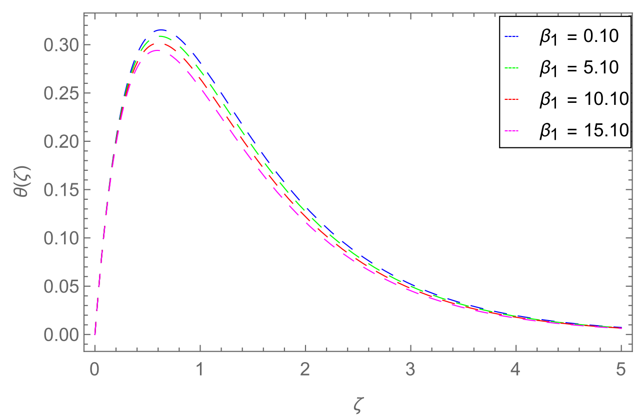

Fig. 26 Behavior of profile against parameter effect

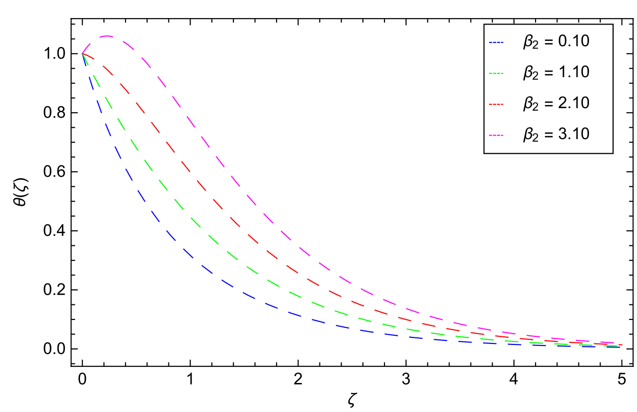

Fig. 27 Behavior of profile against parameter effect

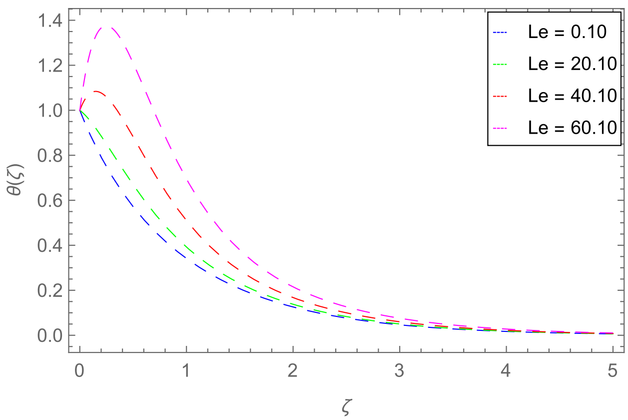

Fig. 28 Behavior of profile against parameter effect

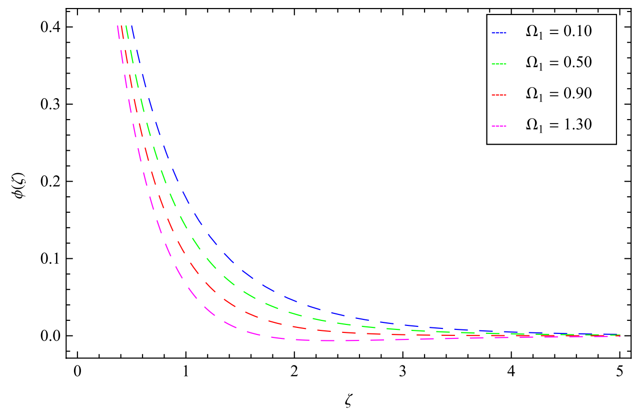

Fig. 31 Behavior of profile against parameter effect

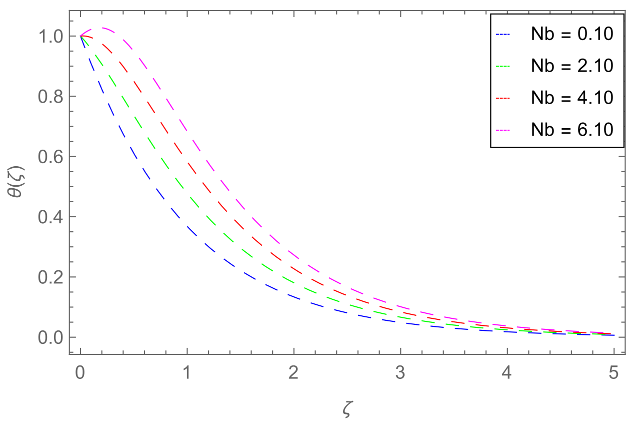

Fig. 29 Behavior of profile against parameter effect

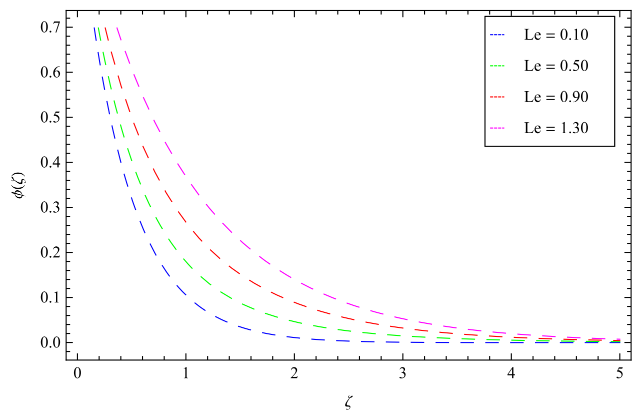

Fig. 32 Behavior of profile against parameter effect

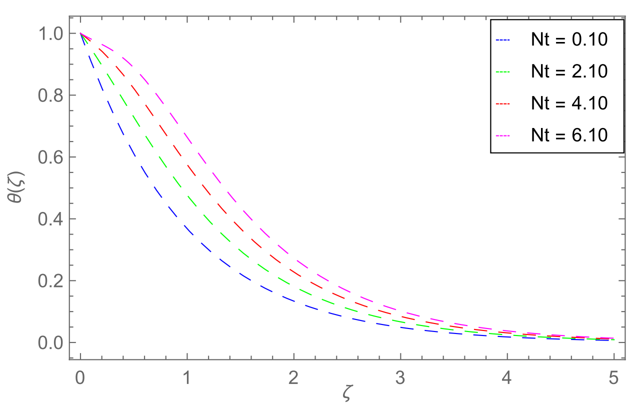

Fig. 30 Behavior of profile against parameter effect

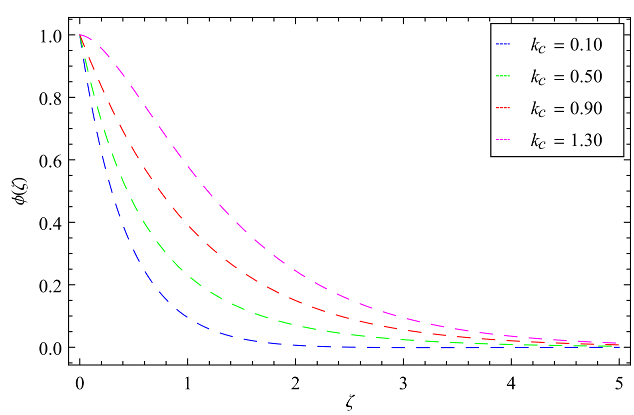

Fig. 33 Behavior of profile against parameter effect

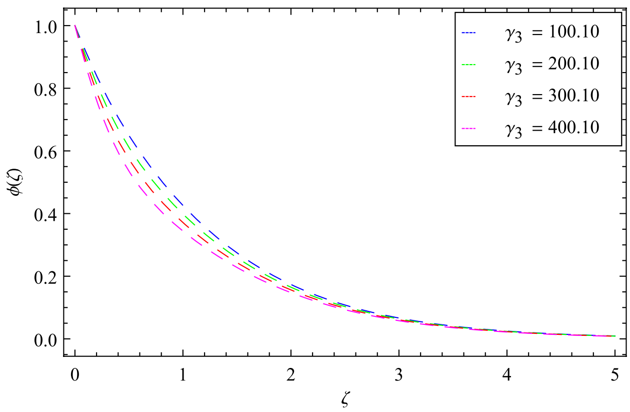

Fig. 34 Behavior of profile against parameter effect

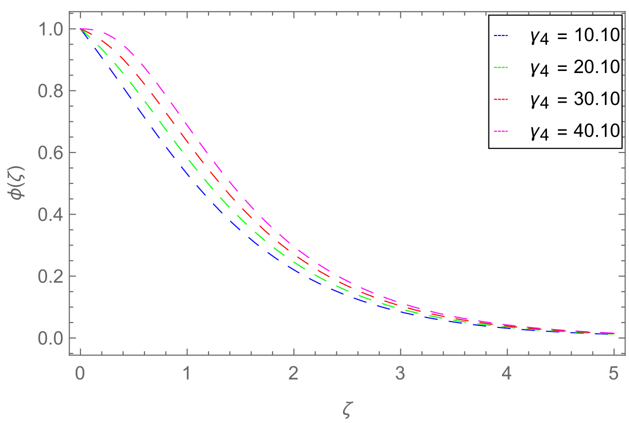

Fig. 35 Behavior of profile against parameter effect

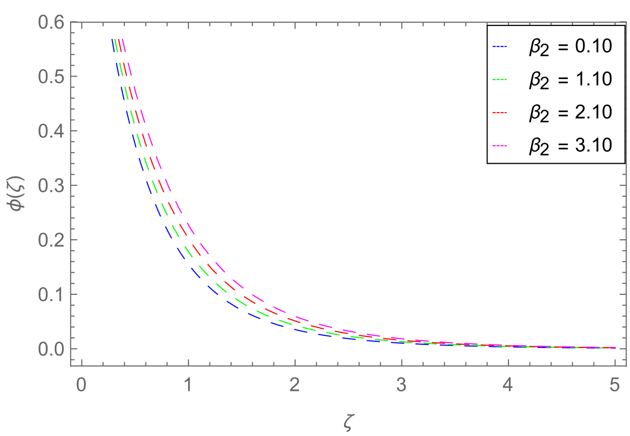

Fig. 36 Behavior of profile against parameter effect

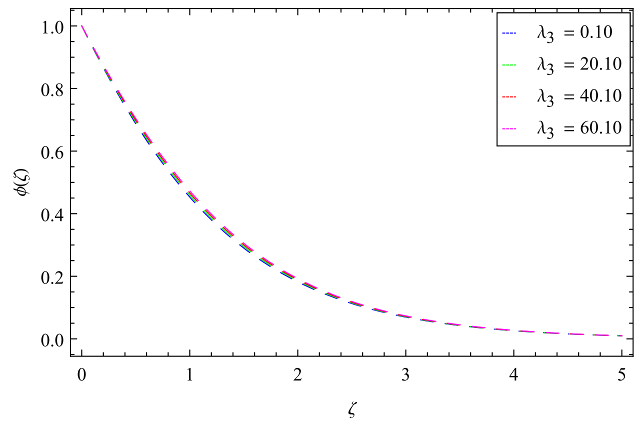

Fig. 37 Behavior of profile against parameter effect

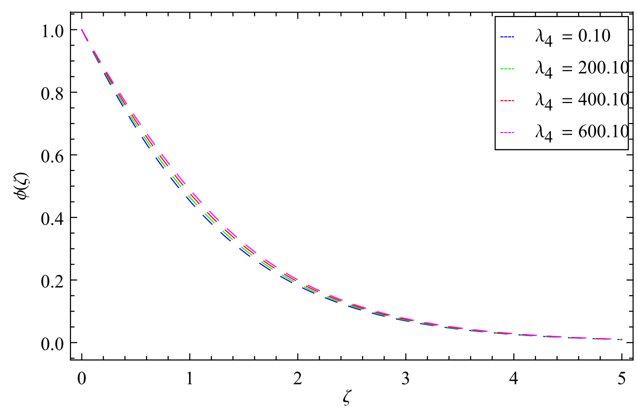

Fig. 38 Behavior of profile against parameter effect

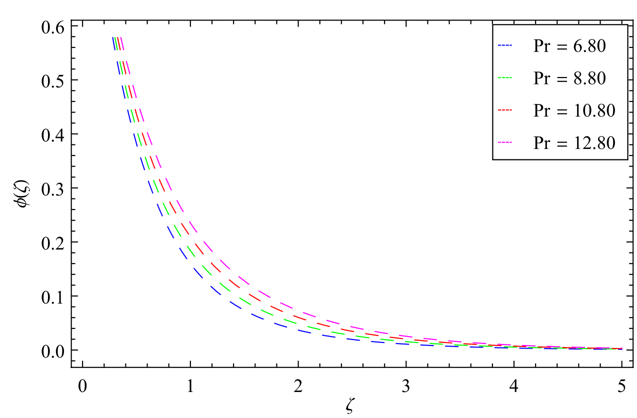

Fig. 39 Behavior of profile against parameter effect

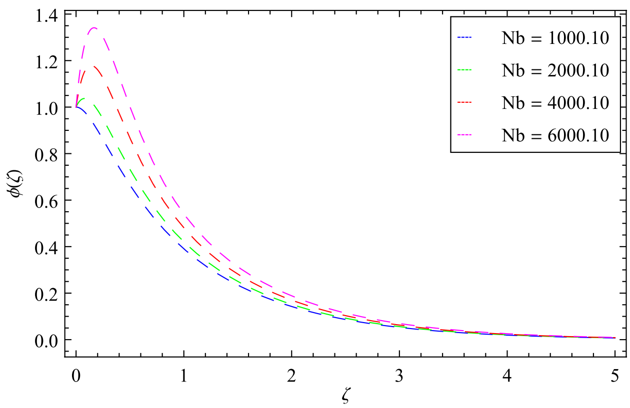

Fig. 40 Behavior of profile against parameter effect

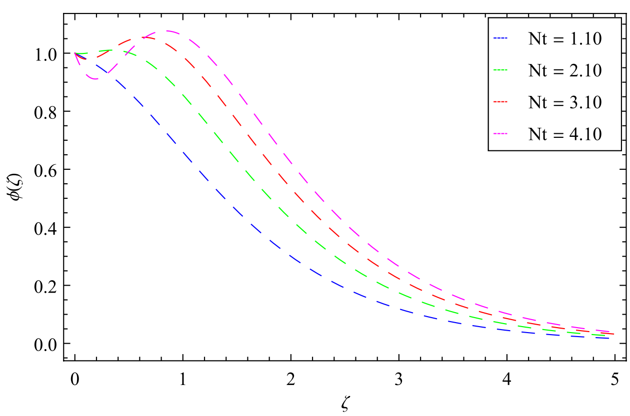

Fig. 41 Behavior of profile against parameter effect

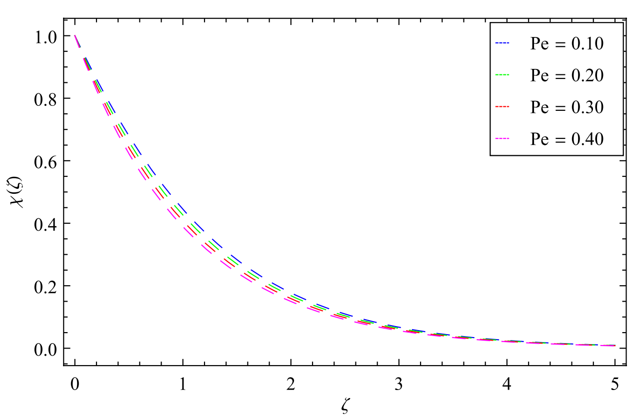

Fig. 42 Behavior of profile against parameter effect

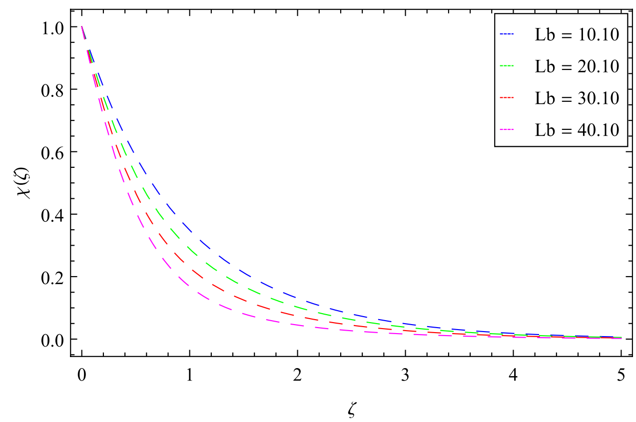

Fig. 43 Behavior of profile against parameter effect

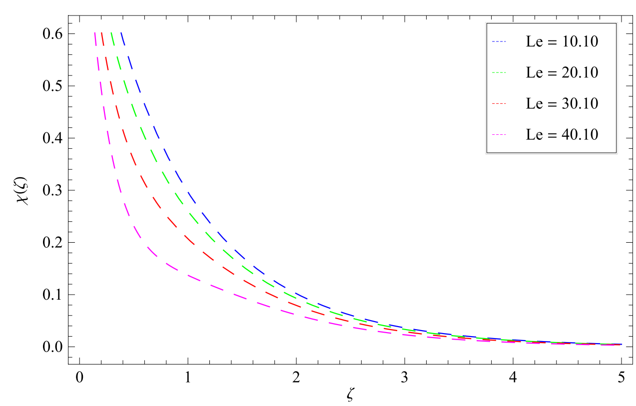

Fig. 44 Behavior of profile against parameter effect

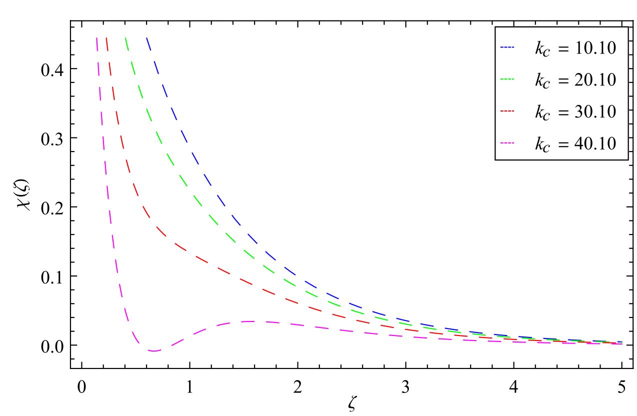

Fig. 45 Behavior of profile against parameter effect

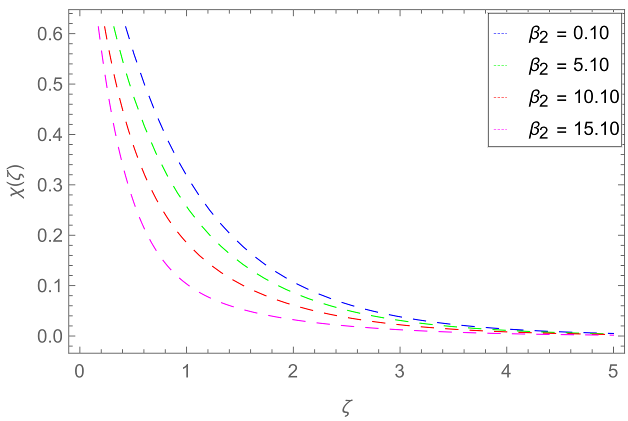

Fig. 46 Behavior of profile against parameter effect

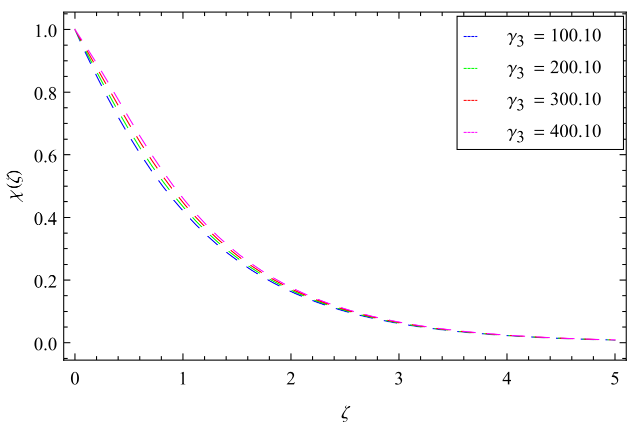

Fig. 47 Behavior of profile against parameter effect

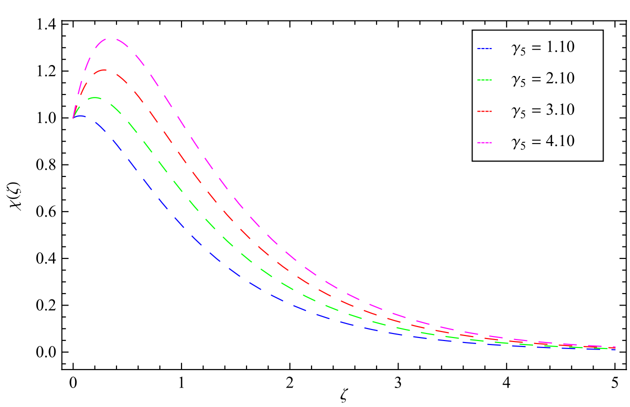

Fig. 48 Behavior of profile against parameter effect

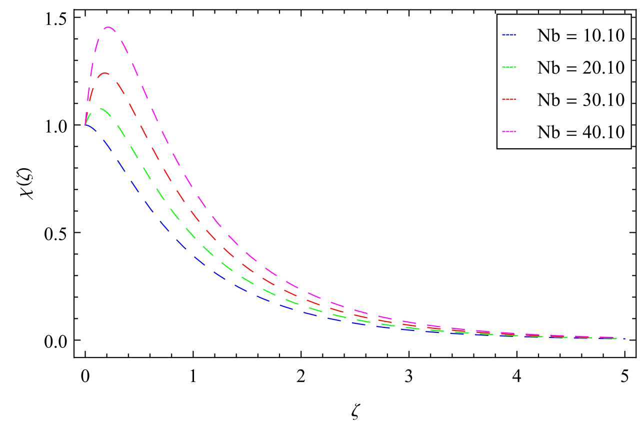

Fig. 49 Behavior of profile against parameter effect

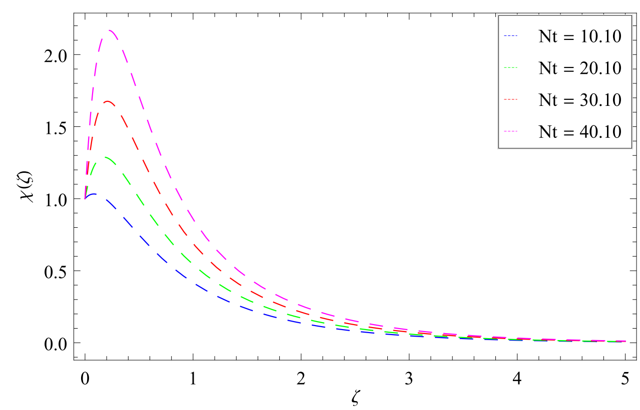

Fig. 50 Behavior of profile against parameter effect

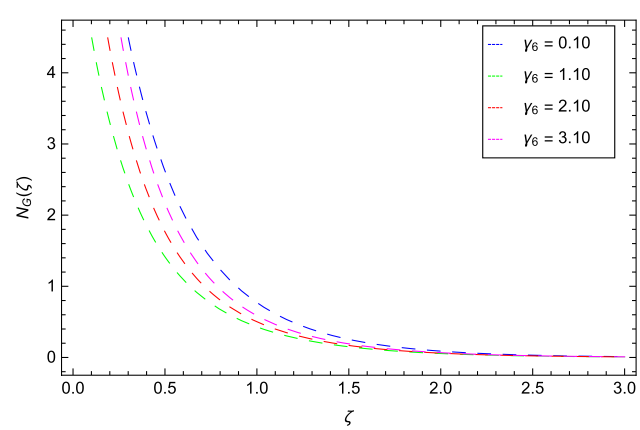

Fig. 51 Behavior of profile against parameter effect

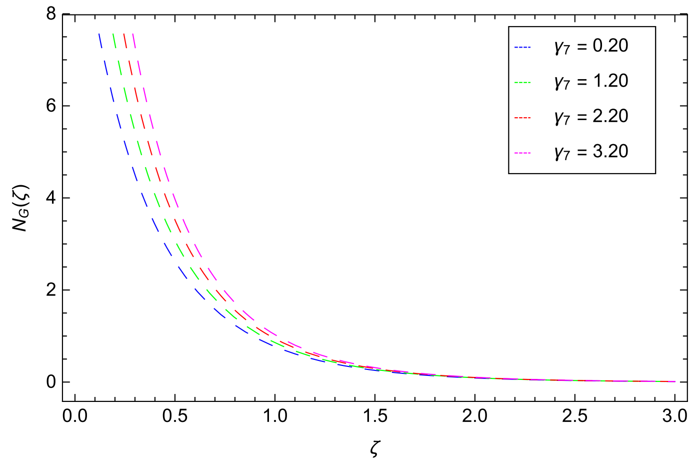

Fig. 52 Behavior of profile against parameter effect

velocity $g(\zeta)$. Fluid motion is reduced by these two parameters (λ_3, λ_4). Figure 11 highlights the effect of Hall parameter m on the azimuthal velocity $g(\zeta)$. It is noted that the velocity component $g(\zeta)$ is made stronger by the given relation $\frac{M(mf' + g - 2\beta_1 hg')}{1 + m^2}$ through Eq. (12). The same mathematical relation $\frac{M(mf' + g - 2\beta_1 hg')}{1 + m^2}$ also supports the azimuthal velocity $g(\zeta)$ for the magnetic field parameter M as it is evident from Fig. 12. The status of azimuthal velocity $g(\zeta)$ is enhanced with respect to fluid motion for the greater values of Maxwell nanofluid parameter β_1 which is clear from Fig. 13.

The axial velocity $h(\zeta)$ has increasing behaviors for the stretching parameter Ω_1, porosity parameter λ_3, Darcy Forchheimer parameter λ_4, and Hall parameter m represented in Figs. 14, 15, 16, and 17 respectively. Figures 18 and 19 reflect on the decreasing effects of magnetic field parameter M and Maxwell nanofluid parameter β_1 for the axial velocity $h(\zeta)$ due to resistive behaviors.

Figure 20 is constructed to show the effect of stretching parameter Ω_1 on heat transfer $\theta(\zeta)$. On expansion of the disk, the temperature of the disk is reduced. The impact of Prandtl number Pr on temperature $\theta(\zeta)$ is given in Fig. 21. The figure shows a reducing behavior of heat transfer of Maxwell nanofluid by assuming different values of Prandtl number. In fact, for the high values of Prandtl number, the thermal diffusion is low; consequently, the fall in the heat transfer is occurred. In Figs. 22 and 23, it is observed that for the larger values of porosity and Darcy Forchheimer parameters (λ_3, λ_4), the expansion of temperature distribution $\theta(\zeta)$ is noted. The influence of thermal relaxation time parameter γ_3 on temperature $\theta(\zeta)$ is portrayed in Fig. 24. Both the thermal boundary layer and heat transfer are increased when the value of thermal relaxation time parameter γ_3 is increased. Physically, for the increasing values of γ_3, the particles of fluid transfer more heat to adjacent particles. Figure 25 is plotted to show the effect of chemical reaction parameter k_c on heat transfer $\theta(\zeta)$. For the higher values of k_c, the concentration is increased which increases the temperature. Figure 26 displays the behaviors of Maxwell nanofluid parameter β_1 and temperature profile $\theta(\zeta)$. The temperature boundary layer is decreased because more heat is required for the particles of Maxwell nanofluid due to its viscosity. The role of heat generation parameter β_2 is discussed in Fig. 27. Clearly, $\theta(\zeta)$ boosts up for the larger values of β_2 since the heat source/sink coefficient is increased. It is due to the fact that heat source/sink parameter β_2 creates an extra heat in the fluid. Figure 28 demonstrates the significance of Lewis number Le and heat transfer $\theta(\zeta)$. It is clear that temperature is an increasing function of Le. Figure 29 depicts the result that with higher estimates of Brownian motion parameter Nb, the non-dimensional temperature $\theta(\zeta)$ is increased. In fact, with the rise of Nb, Brownian motion of the fluid particles increases which generates resistance to the mass transport and increases the heat. Figure 30 indicates that temperature $\theta(\zeta)$ is improved with higher values of thermophoresis parameter Nt. It is due to the fact that greater values of Nt enhance the thermophoretic force which results in increment in heat transport.

Figure 31 captures the decrease of nanoparticles concentration $\phi(\zeta)$ due to stretching parameter Ω_1. Figures 32 and 33 depict the features of Lewis number Le and chemical reaction parameter k_c respectively. It is recognized that for the higher estimations of Le and k_c, the nanoparticles concentration $\phi(\zeta)$ is enhanced. Figure 34 scrutinizes the influence of thermal relaxation time parameter γ_3 on nanoparticles concentration $\phi(\zeta)$. Physically, with rise of γ_3, the increase in the relaxation time is occurred which decreases the mass transport. The characteristics of the non-dimensional solutal relaxation time parameter γ_4 and nanoparticles concentration profile $\phi(\zeta)$ are seen in Fig. 35. An increment in γ_4 causes high concentration between the fluid and nanoparticles. The reason is that with increasing values of solutal relaxation time parameter, the propagation of concentration layers is enhanced which increases the mass transport. Similarly, in Fig. 36, it is noted that the nanoparticles concentration $\phi(\zeta)$ is maximum with increasing values of heat source/sink parameter β_2 because the extra heat provides more conversion to high concentration. Figures 37, 38, 39, 40, and 41 illustrate the effects of porosity parameter λ_3, Darcy Forchheimer parameter λ_4, Prandtl number Pr, Brownian motion parameter Nb, and thermophoresis parameter Nt respectively on nanoparticles concentration $\phi(\zeta)$. It is interpreted that $\phi(\zeta)$ attains maximum value for all these parameter estimations.

Figure 42 characterizes that the high values of Peclet number Pe lead to the reduction of gyrotactic microorganisms concentration $\chi(\zeta)$. It is clearly shown that the Peclet number Pe is very closely related to gyrotactic microorganisms concentration $\chi(\zeta)$ and nanoparticles concentration $\phi(\zeta)$ written in Eq. (15), i.e., $\chi'' - Lbh\chi' - Pe\left(\chi'\phi' + \phi''(\gamma_5 + \chi)\right) = 0$. Similarly in Fig. 43, it is observed that the various values of bioconvection Lewis number Lb lead to the minimum value of gyrotactic microorganisms concentration $\chi(\zeta)$ which is also evident from Eq. (15). Figures 44, 45, and 46 are delineated to show the effects of Lewis number Le, chemical reaction parameter k_c, and the heat source/sink parameter β_2 on the gyrotactic microorganisms concentration $\chi(\zeta)$ respectively. Due to these parameters, the motion of gyrotactic microorganisms is decreased. Figure 47 indicates that the flow of gyrotactic microorganisms is enhanced by the increasing values of thermal relaxation time parameter γ_3 since time relaxation is provided. The result of microorganisms concentration difference parameter γ_5 is revealed through Fig. 48. Strong microorganisms concentration ultimately uplifts the $\chi(\zeta)$. In Fig. 49, $\chi(\zeta)$ is the increasing function of Brownian motion parameter Nb. Figure 50 indicates that the thermophoresis parameter Nt increases the microorganisms concentration $\chi(\zeta)$ profile.

Figure 51 elucidates the better performance of entropy generation rate $N_G(\zeta)$ due to temperature difference parameter γ_6. The irreversibility of the present system is reduced. In Fig. 52, the result of increasing different values of diffusion constant parameter due to nanoparticles concentration γ_7 is indicated. Enhancement is observed due to γ_7.

7 Conclusions

The Cattaneo-Christov heat and mass flux model is proposed taking into account the Maxwell nanofluid flow in a porous medium with gyrotactic microorganisms, entropy generation, and Hall current effect for the spinning disk. The homotopy analysis method (HAM) is applied for the computation of transformed equations resulting through similarity transformation. Heat and mass transfer are enhanced due to Cattaneo-Christov heat and mass flux model.

The main results are summarized as follows.

(1) The radial velocity is reduced with the increasing values of Hall, Maxwell nanofluid, and magnetic field parameters while it is enhanced with porosity, Darcy Forchheimer, and stretching parameters.
(2) The azimuthal velocity is reduced with the increasing values of stretching, porosity, and Darcy Forchheimer parameters while it is enhanced with the increasing values of Hall, Maxwell nanofluid, and magnetic field parameters.
(3) The axial velocity is reduced with the increasing values of Maxwell nanofluid and magnetic field parameters while it is enhanced with porosity, Darcy Forchheimer, Hall, and stretching parameters.
(4) The temperature is reduced with the increasing values of Prandtl number, stretching, Maxwell nanofluid, and chemical reaction parameters while it is enhanced with porosity, Darcy Forchheimer, thermal relaxation time, heat source/sink, Brownian motion, thermophoresis parameters, and Lewis number.
(5) The nanoparticles concentration is reduced with the increasing values of stretching and thermal relaxation time parameters and Schmidt number while it is enhanced with Lewis and Prandl numbers, chemical reaction, the porosity, Darcy Forchheimer, solutal relaxation time, heat source/sink, Brownian motion, and thermophoresis parameters.
(6) The gyrotactic microorganisms concentration is reduced with the increasing values of Peclet, bioconvection Lewis and Lewis numbers, chemical reaction, and heat source/sink parameters while it is enhanced with the increasing values of thermal relaxation time, thermophoresis, gyrotactic microorganisms concentration difference, and Brownian motion parameters.
(7) Entropy generation is reduced with temperature difference parameter while it is enhanced with values of diffusion constant parameter due to nanoparticles concentration.
(8) Numerical comparison with published work provides a nice agreement.

Acknowledgements The authors are thankful to the respectable reviewers for their comments and suggestions. The authors acknowledge the financial support provided by the Center of Excellence in Theoretical and Computational Science (TaCS-CoE), KMUTT. Moreover, this research was supported by The Science, Research and Innovation Promotion Funding (TSRI) (Grant no. FRB650070/0168). This research block grants was managed under Rajamangala University of Technology Thanyaburi (FRB65E0633M.2). The authors extend their appreciation to the Deanship of Scientific Research at King Khalid University, Abha, Saudi Arabia for funding this work through research groups program under grant number RGP.1/248/43.The first author is thankful to the Higher Education Commission (HEC) Pakistan for funding through the SRGP project No. 10534.

Author contribution All authors contributed to the study conception and design. Conceptualization: Noor Saeed Khan, methodology: Poom Kumam, formal analysis: Usa Wannasingha Humphries, investigation: Wiyada Kumam, resources: Noor Saeed Khan, supervision: Taseer Muhammad, writing—original draft: Taseer Muhammad, writing—review and editing: Noor Saeed Khan.

Data availability Upon reasonable request to the corresponding author, the data will be provided.

Declarations

Conflict of interest The authors declare no competing interests.

References

1. Wang F, Rehman S, Bouslimi J, Khaliq H, Qureshi MI, Kamran M, Alharbi AN, Ahmad H, Farooq A (2021) Comparative study of heat and mass transfer of generalized MHD Oldroyd-B bio-nano fluid in a permeable medium with ramped conditions. Sci Rep 11:23454. https://doi.org/10.1038/s41598-021-02326-8
2. Farooq U, Waqas H, Khan MI, Khan SU, Chu YM, Kadry S (2021) Thermally radioactive bioconvection flow of Carreau nanofluid with modified Cattaneo-Christov expressions and exponential space-based heat source. Alex Eng J 60:3073–3086. https://doi.org/10.1016/j.aej.2021.01.050
3. Alzahrani J, Vaidya H, Prasad KV, Rajashekhar C, Mahendra DL, Tlili I (2022) Micropolar fluid flow over a unique form of vertical stretching sheet: special emphasis to temperature-dependent properties. Case Stud Therm Eng 34:102037. https://doi.org/10.1016/j.csite.2022.102037
4. Ahmad S, Nadeem S, Khan MN (2022) Heat enhancement analysis of the hybridized micropolar nanofluid with Cattaneo-Christov and stratification effects. J Mech Eng Sci 234(2):943–955. https://doi.org/10.1177/09544062211010833
5. Song YQ, Farooq A, Kamran M, Rehman S, Tamoor M, Khan R, Fahad A, Qureshi MI (2021) Analytical solution of fractional Oldroyd-B fluid via fluctuating duct. Complexity 2021(9576873):1–16. https://doi.org/10.1155/2021/9576873
6. Almutairi B, Kamran M, Farooq A, Ahmad H, Shahzad A, Khan FU, Khan AS, Almohsen B (2022) On the Taylor-Couette flow of fractional oldroyd-B fluids in a cylindrically symmetric configuration using transforms. Int J Modern Phys C. https://doi.org/10.1142/S0129183122500991
7. Tlili I, Sajadi SM, Baleanu D, Ferial Ghaemi F (2022) Flat sheet direct contact membrane distillation study to decrease the energy demand for solar desalination purposes. Sustain Energy Technol Assess 52:102100. https://doi.org/10.1016/j.seta.2022.102100
8. Zhanga J, Sajadi SM, Chen Y, Tlili I, Fagirye MA (2022) Effects of Al_2O_3 and TiO_2 nanoparticles in order to reduce the energy demand in the conventional buildings by integrating the solar collectors and phase change materials. Sustain Energy Technol Assess 52:102114. https://doi.org/10.1016/j.seta.2022.102114
9. Tlili I, Alharbi T (2022) Investigation into the effect of changing the size of the air quality and stream to the trombe wall for two different arrangements of rectangular blocks of phase change material in this wall. J Building Eng 52:104328. https://doi.org/10.1016/j.jobe.2022.104328
10. Qia X, Sidi MO, Tlili T, Ibrahim TK, Elkotb MA, El-Shorbagy MA, Li Z (2022) Optimization and sensitivity analysis of extended surfaces during melting and freezing of phase changing materials in cylindrical Lithium-ion battery cooling. J Energy Storage 51:104545. https://doi.org/10.1016/j.est.2022.104545
11. Gao J, Liu J, Yue H, Zhao Y, Tlili I, Karimipour A (2022) Effects of various temperature and pressure initial conditions to predict the thermal conductivity and phase alteration duration of water based carbon hybrid nanofluids via MD approach. J Mol Liquid 351:118654. https://doi.org/10.1016/j.molliq.2022.118654
12. Mahmood RT, Asad MJ, Hadri SH, El-Shorbagy MA, Mousa AAA, Dara RN, Awais M, Tlili I (2022) Bioremediation of textile industrial effluents by Fomitopsis pinicola IEBL-4 for environmental sustainability. Human Ecol Risk Assess: An Int J 351:1–18. https://doi.org/10.1080/10807039.2022.2057277
13. Nayak MK, Mabood F, Dogonchi AS, Ramadan KM, Tlili I, Khan WA (2022) Entropy optimized assisting and opposing non-linear radiative flow of hybrid nanofluid. Waves Random Complex Media 1–22. https://doi.org/10.1080/17455030.2022.2032474
14. Ramadan KM, Qisieh O, Tlili I (2022) Thermal creep effects on fluid flow and heat transfer in a microchannel gas cooling. J Mech Eng Sci 236(9):5033–5047. https://doi.org/10.1177/09544062211057039
15. Khan MN, Ahmad S, Ahammad NA, Alqahtani T, Algarni S (2022) Numerical investigation of hybrid nanofluid with gyrotactic microorganism and multiple slip conditions through a porous rotating disk. Waves Random Complex Media 1–16. https://doi.org/10.1080/17455030.2022.2055205
16. Ahmad S, Khan MN, Nadeem S (2022) Numerical investigation of hybrid nanofluid with gyrotactic microorganism and multiple slip conditions through a porous rotating disk. Int J Ambient Energy 1–11. https://doi.org/10.1080/01430750.2022.2029765
17. Ahmad S, Nadeem S (2021) Hybridized nanofluid with stagnation point past a rotating disk. Phys Scr 96:025214. https://doi.org/10.1088/1402-4896/abcfef
18. Ahmad S, Nadeem S, Khan MN (2021) Mixed convection hybridized micropolar nanofluid with triple stratification and Cattaneo-Christov heat flux model. Phys Scr 96:075205. https://doi.org/10.1088/1402-4896/abf615
19. Khan NS, Shah Q, Sohail A (2020) Dynamics with Cattaneo-Christov heat and mass flux theory of bioconvection Oldroyd-B nanofluid. Adv Mech Eng 12(7):1–20. https://doi.org/10.1177/1687814020930464
20. Irfan M, Khan M, Gulzar MM, Khan WA (2020) Chemically reactive and nonlinear radiative heat flux in mixed convection flow of Oldroyd-B nanofluid. Appl Nanosci 10:3133–3141. https://doi.org/10.1007/s13204-019-01052-y
21. Khan M, Irfan M, Khan W, Sajid M (2019) Consequence of convective conditions for flow of Oldroyd-B nanofluid by a stretching cylinder. J Braz Soci Mech Sci Eng 41:116. https://doi.org/10.1007/s40430-019-1604-3
22. Irfan M, Khan M, Khan WA (2019) Impact of non-uniform heat sink source and convective condition in radiative heat transfer to Oldroyd-B nanofluid: a revised proposed relation. Phys Letters A 383(4):376–382. https://doi.org/10.1016/j.physleta.2018.10.040
23. Hafeez A, Khan M, Ahmed J, Ahmed J (2020) Rotational flow of Oldroyd-B nanofluid subject to Cattaneo-Christov double diffusive theory. Appl Math Mech Engl Ed 41(7):1083–1094. https://doi.org/10.1007/s10483-020-2629-9
24. Usman AH, Khan NS, Humphries UW, Ullah Z, Shah Q, Kumam P, Thounthong P, Khan W, Kaewkhao Bhaumik (2021) Computational optimization for the deposition of bioconvection thin Oldroyd-B nanofluid with entropy generation. Sci Rep 11(1):11641. https://doi.org/10.1038/s41598-021-91041-5
25. Khan N, Hashmi MS, Khan SU, Chaudhery F, Tlili I, Shadloo MS (2020) Effects of homogeneous and heterogeneous chemical features on Oldroyd-B fluid flow between stretching disks with velocity and temperature boundary assumptions. Math Prob Eng 2020:5284906. https://doi.org/10.1155/2020/5284906
26. Hashmi MS, Khan N, Khan SU, Rashidi MM (2017) A mathematical model for mixed convective flow of chemically reactive

Oldroyd-B fluid between isothermal stretching disks. Res Phys 7:3016–3023. https://doi.org/10.1016/j.rinp.2017.08.017
27. Tong ZW, Khan SU, Vaidya H, Rajashekhar R, Sun TC, Khan MI, Prasad KV, Chinram R, Aly AA (2021) Nonlinear thermal radiation and activation energy significances in slip flow of bioconvection of Oldroyd-B nanofluid with with Cattaneo-Christov theories. Case Stud Therm Eng 26:101069. https://doi.org/10.1016/j.csite.2021.101069
28. Hashmi MS, Khan N, Khan SU, Khan MI, Khan NB, Nazeer M, Kadry S, Chu YM (2021) Dynamics of coupled reacted flow of Oldroyd-B material induced by isothermal/exothermal stretched disks with Joule heating, viscous dissipation and magnetic dipoles. Alex Eng J 60(1):767–783. https://doi.org/10.1016/j.aej.2020.10.007
29. Irfan M, Khan M, Khan WA (2018) On model for three-dimensional Carreau fluid flow with Cattaneo-Christov double diffusion and variable conductivity: a numerical approach. J Braz Soci Mech Sci Eng 40:577. https://doi.org/10.1007/s40430-018-1498-5
30. Irfan M, Khan M, Muhammad T, Waqas M, Khan WA (2022) Analysis of energy transport considering Arrhenius activation energy and chemical reaction in radiative Maxwell nanofluid flow. Chem Phys Letter 793:139323. https://doi.org/10.1016/j.cplett.2021.139323
31. Irfan M (2021) Study of Brownian motion and thermophoretic diffusion on non-linear mixed convection flow of Carreau nanofluid subject to variable properties. Surf Interf 23:100926. https://doi.org/10.1016/j.surfin.2021.100926
32. Khan NS, Zuhra S, Shah Z, Bonyah E, Islam S, Khan W, Khan A (2019) Hall current and thermophoresis effects on magnetohydrodynamic mixed convective heat and mass transfer thin film flow. J Phys Commun 3:035009. https://doi.org/10.1088/2399-6528/aaf830
33. Khan NS, Gul T, Islam S, Khan W (2017) Thermophoresis and thermal radiation with heat and mass transfer in a magnetohydrodynamic thin film second-grade fluid of variable properties past a stretching sheet. Eur Phys J Plus 132:11. https://doi.org/10.1140/epjp/i2017-11277-3
34. Khan NS, Gul T, Kumam P, Shah Z, Khan W, Islam S, Zuhra S, Sohail A (2019) Influence of inclined magnetic field on Carreau nanoliquid thin film flow and heat transfer with graphene nanoparticles. Energies 12:1459. https://doi.org/10.3390/en12081459
35. Waqas H, Hussain M, Alqarnib MS, Eid MR, Muhammad T (2021) Numerical simulation for magnetic dipole in bioconvection flow of Jeffrey nanofluid with swimming motile microorganisms. Waves Random Complex Media 1–18. https://doi.org/10.1080/17455030.2021.1948634
36. Raja MAZ, Khan Z, Zuhra S, Chaudhary NI, Khan WU, He Y, Islam S, Shoaib M (2021) Cattaneo-Christov heat flux model of 3D hall current involving bioconvection nanofluidic flow with Darcy-Forchheimer law effect: backpropagation neural networks approach. Case Stud Therm Eng 26:101168. https://doi.org/10.1016/j.csite.2021.101168
37. Waqas H, Imran M, Muhammad T, Salt SM, Ellahi R (2021) Numerical investigation on bioconvection flow of Oldroyd-B nanofluid with non-linear thermal radiation and motile microorganisms over rotating disk. J Therm Anal Calor 145:523–539. https://doi.org/10.1007/s10973-020-09728-2
38. Khan NS, Shah Q, Sohail A, Kumam P, Thounthong P, Muhammad T (2021) Mechanical aspects of Maxwell nanofluid in dynamic system with irreversible analysis. Z Angew Math Mech 8:e202000212. https://doi.org/10.1002/zamm.202000212
39. Khan NS, Kumam P, Thounthong P (2019) Renewable energy technology for the sustainable development of thermal system with entropy measures. Int J Heat Mass Transf 145:118713. https://doi.org/10.1016/j.ijheatmasstransfer.2019.118713
40. Khan NS (2018) Bioconvection in second grade nanofluid flow containing nanoparticles and gyrotactic microorganisms. Braz J Phys 43:227–241. https://doi.org/10.1007/s13538-018-0567-7
41. Khan NS, Gul T, Khan MA, Bonyah E, Islam S (2017) Mixed convection in gravity-driven thin film non-Newtonian nanofluids flow with gyrotactic microorganisms. Result Phys 7:4033–4049. https://doi.org/10.1016/j.rinp.2017.10.017
42. Khan NS (2019) Mixed convection in MHD second grade nanofluid flow through a porous medium containing nanoparticles and gyrotactic microorganisms with chemical reaction. Filomat 33:4627–4653. https://doi.org/10.2298/FIL1914627K
43. Khan NS, Shah Z, Shutaywi M, Kumam P, Thounthong P (2020) A comprehensive study to the assessment of Arrhenius activation energy and binary chemical reaction in swirling flow. Sci Rep 10:7868. https://doi.org/10.1038/s41598-020-64712-y
44. Ramesha K, Khan SU, Jameel M, Khan MI, Chu YM, Kadry S (2020) Bioconvection assessment in Maxwell nanofluid configured by a Riga surface with nonlinear thermal radiation and activation energy. Surf Interf 21:100749. https://doi.org/10.1016/j.surfin.2020.100749
45. Liu C, Khan MU, Ramzan M, Chu YM, Kadry S, Malik MY, Chinram R (2021) Nonlinear radiative Maxwell nanofluid flow in a Darcy-Forchheimer permeable media over a stretching cylinder with chemical reaction and bioconvection. Sci Rep 11:9391. https://doi.org/10.1038/s41598-021-88947-5
46. Ramzan M, Gul H, Kadry S, Chu YM (2021) Role of bioconvection in a three dimensional tangent hyperbolic partially ionized magnetized nanofluid flow with Cattaneo-Christov heat flux and activation energy. Int Commun Heat Mass Transf 120:104994. https://doi.org/10.1016/j.icheatmasstransfer.2020.104994
47. Song YQ, Khan SA, Imran M, Waqas H, Khan SU, Khan MI, Qayyum S, Chu YM (2021) Applications of modified Darcy law and nonlinear thermal radiation in bioconvection flow of micropolar nanofluid over an off centered rotating disk. Alex Eng J 60:4607–4618. https://doi.org/10.1016/j.aej.2021.03.053
48. Song YQ, Waqas H, Al-Khaled K, Farooq M, Khan SU, Khan MI, Chu YM, Qayyum S (2021) Bioconvection analysis for Sutterby nanofluid over an axially stretched cylinder with melting heat transfer and variable thermal features: a Marangoni and solutal model. Alex Eng J 60:4663–4675. https://doi.org/10.1016/j.aej.2021.03.056
49. Abdal S, Siddique I, Afzal S, Chu YM, Ahmadian A, Salahshour S (2021) On development of heat transportation through bioconvection of Maxwell nanofluid flow due to an extendable sheet with radiative heat flux and prescribed surface temperature and prescribed heat flux conditions. Math Meth Appl Sci 1–18. https://doi.org/10.1002/mma.7722
50. Chu YM, Rahman MU, Khan MI, Kadry S, Rehman WU, Abdelmalek Z (2021) Heat transport and bio-convective nanomaterial flow of Walter's-B fluid containing gyrotactic microorganisms. Ain Shams Eng J 12(3):3071–3079. https://doi.org/10.1016/j.asej.2020.10.025
51. Zhao TH, Khan MI, Chu YM (2020) Artificial neural networking (ANN) analysis for heat and entropy generation in flow of non-Newtonian fluid between two rotating disks. Math Meth Appl Sci 1–19. https://doi.org/10.1002/mma.7310
52. Shah F, Khan MI, Chu YM, Kadry S (2020) Heat transfer analysis on MHD flow over a stretchable Riga wall considering entropy generation rate: a numerical study. Num Methods Partial Differential Eq 1–17. https://doi.org/10.1002/num.22694
53. Qayyum S, Khan MI, Masood F, Chu YM, Kadry S, Nazeer M (2019) Interpretation of entropy generation in Williamson fluid flow with nonlinear thermal radiation and first-order velocity slip. Math Meth Appl Sci 1–10. https://doi.org/10.1002/mma.6735
54. Khan MI, Qayyum S, Chu YM, Kadry S (2020) Numerical simulation and modeling of entropy generation in Marangoni convective

flow of nanofluid with activation energy. Num Methods Partial Differential Eq 1–11. https://doi.org/10.1002/num.22610
55. Khan NS, Zuhra S, Shah Q (2019) Entropy generation in two phase model for simulating flow and heat transfer of carbon nanotubes between rotating stretchable disks with cubic autocatalysis chemical reaction. Appl Nanosci 9:1797–1822. https://doi.org/10.1007/s13204-019-01017-1
56. Khan NS, Shah Q, Bhaumik A, Kumam P, Thounthong P, Amiri I (2020) Entropy generation in bioconvection nanofluid flow between two stretchable rotating disks. Sci Rep 10:4448. https://doi.org/10.1038/s41598-020-61172-2
57. Khan NS, Shah Z, Islam S, Khan I, Alkanhal TA, Tlili I (2019) Entropy generation in MHD mixed convection non-Newtonian second-grade nanoliquid thin film flow through a porous medium with chemical reaction and stratification. Entropy 21:139. https://doi.org/10.3390/e21020139
58. Usman AH, Khan NS, Rano SA, Humphries UW, Kumam P (2021) Computational investigations of Arrhenius activation energy and entropy generation in a viscoelastic nanofluid flow thin film sprayed on a stretching cylinder. J Adv Res Fluid Mech Therm 86(1):27–51. https://doi.org/10.37934/arfmts.86.1.2751
59. Ramzan M, Khan NS, Kumam P (2021) Mechanical analysis of non-Newtonian nanofluid past a thin needle with dipole effect and entropic characteristics. Sci Rep 11(1):19378. https://doi.org/10.1038/s41598-021-98128-z
60. Khan NS, Humphries UW, Kumam W, Kumam P, Muhammad T (2022) Bioconvection Casson nanoliquid film sprayed on a stretching cylinder in the portfolio of homogeneous-heterogeneous chemical reactions. Z Angew Math Mech 8:e2020000222. https://doi.org/10.1002/zamm.202000212
61. Shijun L (2004) On the homotopy analysis method for non-linear problems. Appl Math Comput 147(2):499–513. https://doi.org/10.1016/S0096-3003(02)00790-7
62. Ahmed A, Khan M, Ahmed J, Hafeez A (2020) Von Karman rotating flow of Maxwell nanofluids featuring the Cattaneo-Christov theory with a Buongiorno model. Appl Math Mech -Engl Ed 41(8):1195–1208. https://doi.org/10.1007/s10483-020-2632-8